Study of Deposition Strategies of a Wire + Arc Additive Manufactured Component

Maria Inês Castro e Silva

ines.castro@ist.utl.pt

[*] Mechanical and Materials Engineering Department, Instituto Superior Técnico, Universidade de Lisboa, Portugal

ABSTRACT

Fabrication of metal parts by wire and arc additive manufacturing (WAAM) has received an increased interest in recent years, as it allows high design flexibility and reduction of material wastage as compared to other traditional manufacturing routes. In this study, a bulk complex structure was made by different deposition strategies, in wire and arc additive manufacturing (WAAM), using aluminium 2319, to understand the influence of deposition strategies in porosity, microstructure, microhardness, path efficiency and substrate deformation. Samples were built by using different oscillation deposition paths with alternating current plasma arc welding power source (ACPAW). This technology is a relatively new and promising for welding aluminium due to its efficient oxide cleaning capability and reduction of porosity when compared to the cold metal transfer process. A WAAM software, being developed by Cranfield University, was employed efficiently to program the chosen tool paths. The deposited parts displayed similar microhardness results which were consistent with the achieved microstructure. The average pore diameter size for the deposition strategies was in the range of 16.2 μm to 25.7 μm. The most suitable deposition strategy for the part in study was proposed. Additionally, the substrate deformation results showed that the deposition strategies will have an influence on the residual stresses distribution. It has been shown that using an ACPAW power source for deposition of WAAM meter scale parts of aluminium alloys can be achieved.

Keywords: AA2319, alternating current plasma arc welding, aluminium alloy, complex geometry, deposition paths, microhardness, microstructure, optimization methods, oscillation strategy, part efficiency, porosity, WAAM software, wire and arc additive manufacturing.

1 INTRODUCTION

AM produces (near-) net shape components by adding layers of material on top of a base plate/substrate with each layer being a cross-section of a CAD (computer-aided design) project [4, 7].

WAAM combines a metal wire feedstock and an electric arc and its hardware is composed by welding machinery (torches, wire feeders, shielding gas and power sources) and a motion system machine [11], allowing a construction of the part layer by layer. A variety of materials are suitable for this type of additive manufacturing technology, such as aluminium, titanium, steel alloys and Inconel®. As aluminium alloys display good properties of strength per weight ratio, the demand from, mainly, the aeronautic and automotive industry has increased the development of this metal alloy in WAAM technology. However, there are some metallurgical problems encountered when depositing aluminium. These are porosity (mainly provided by hydrogen entrapment), quality of the feeding wire (it may influence the corrosion resistance, liquidus and solidus temperatures, microstructure, mechanical properties and porosity appearance), oxide inclusions, sufficient oxide cleaning and loss of alloying elements (of low-melting point elements) [66].

ACPAW has showed better results in producing aluminium deposition, as improves the flexibility of manipulation, adjustments and decreases porosity formation, when compared to other WAAM processes [5, 6]. This technology uses a non-consumable tungsten electrode to produce the weld and has the wire feeding system external to the torch [31, 32]. Alternating current results in a fast deterioration of the electrode due to the high current used. However, it is necessary to use this alternate polarity when welding aluminium since a square wave form gives a suitable balance between the positive and negative current forms, necessary to melt and remove the oxide layer [31].

WAAM research studies have been more focused in simple structures. However, the engineering components required by the industry are more intricate and a research on these types

of structures is necessary [9]. Therefore, when the wall width required is larger than the one achieved by single depositions, the most used deposition strategies for complex structures is the parallel and the oscillation paths, as shown in Figure 1. The oscillated has continuum deposition, resulting in a higher heat accumulation, that promotes fusion between the welds and increases the deposition rate and allows the change of wall with by simply changing the oscillation width. However, when compared to parallel paths, the surface roughness is increased [19].

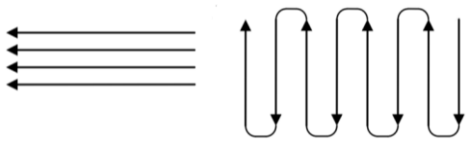

Figure 1: Deposition path strategies. (a) Parallel wall and (b) Oscillated wall strategy [46].

Challenges to include the WAAM manufacturing parts commercially, are related to the existence of residual stresses due to high heat inputs [9], defects (e.g. distortion, porosity) and further study necessary on control of bead geometry, shortage of commercial systems, lack of guidelines and software tools for deposition planning and high expertise demand.

Therefore, building strategies studies are crucial for the development of WAAM in order to take the next step into the industrial sector and to understand the intersections in complex components. Thus, tool-path planning will influence the final product, the efficiency and the mechanical properties [74].

In this context, the present paper aims at studying the influence of deposition strategies in WAAM with ACPAW to build the area highlighted in Figure 2. It will focus on initial deposition parameters optimization, porosity occurrence, cost of part, microscopy observation, microhardness, path efficiency and substrate deformation to contribute to the industrial implementation of this technology.

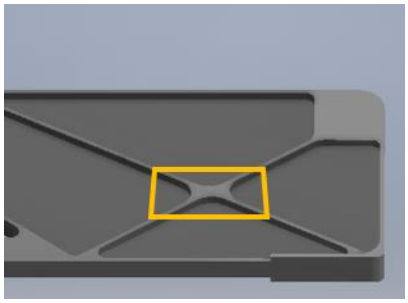

Figure 2 : Part of an aircraft component with the zone of interest highlighted.

2 EXPERIMENTAL METHODS

2.1 Material

The welding consumable wire used throughout the experimental work was the aluminium alloy Böhler-AA2319, with 1.2mm of diameter, as-received. And the substrate material where the geometries were deposited was the aluminium alloy AA6082. The chemical compositions of these metal alloys are available in Table 1.

The substrate plates were cut into the dimension needed (200x200x13 mm^2) to fit the part and ensure enough space for clamping the substrate on the welding table. Posteriorly, they were subjected to a standard surface preparation.

Table 1 : Chemical composition (wt.%) of the materials used [44, 75].

Material	***Composition***										
	Al	Si	Mg	Cr	Mn	Ti	Cu	Zn	Fe	Zr	Other
Filler AA2319	Balance	≤0.2	≤0.02	-	0.2-0.4	0.1-0.2	5.8-6.8	≤0.1	≤0.3	0.1-0.2	≤0.15
Substrate AA6082	Balance	0.7-1.3	0.6-1.2	<0.25	0.4-1	<0.1	<0.1	0.2	<0.5	-	<0.05

2.2 Equipment Set-up

The depositions were accomplished using an ACPAW system composed by a 6-axes KUKA robot, a technical arc wire feeder and a prototype technical AC plasma power source on a steel table where the substrates were clamped. An AMV 4000 machine was utilized to monitor and control the welding voltage and current waveforms as well as the wire feed speed for each of the layers.

3 METODOLOGY

3.1 Parameter optimization and parts deposition

Several preliminary combinations of deposition parameters were studied to generate the most adequate ones to build the part in study, reducing spatter, arc instability and lack of fusion defects. The AC current cycle was maintained as 80% DCEN - 20% DCEP ratio and an overlap area of 66% (see Figure 3) was kept constant to attain a flat surface.

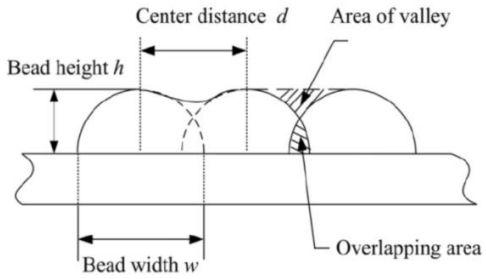

Figure 3: Overlapping welding beads illustration for parallel and oscillation strategies [50].

The shielding gas utilized was argon (99.99%), at a flow rate of 20 L/min, the contact tip to work distance was kept at 8 mm, the wire feed speed at 3.6 m/min and the travel speed at 3 mm/s. The layers were produced by depositing oscillated passes, employing side feeding and alternating direction of deposition in each section. The interlayer cooling temperature was approximately 70ºC and was measured using a thermometer with a temperature probe. Five deposition strategies were manufactured, S1, S2, S3, S4 and S5, for the same geometrical part. On Table 2, it's possible to observe the optimized current values, used on the different deposited layers.

Table 2 : Current values for the different layers, depending on the deposition strategy.

Deposition strategies	Current values, A				
	Layer 1	Layer 2	Layer 3	Layer 4	Layer 5
S1	250	230	200	200	200
S2	250	220	190	180	-
S3	250	230	210	210	210
S4	250	230	210	210	210
S5	250	230	210	210	-

3.2 WAAM Software

The five deposition paths are shown in Figure 4. For the strategies S1-S4, the centre distance was kept in 3.5mm. However, for S5, the distance had to be increased in 1mm, since the 1st layer height reached an average of 8.16mm, which made the weld pool to touch the nozzle and induce a short-circuit. However, to guaranty enough material deposition without lack of fusion, the travel speed was decreased to 2.5 mm/s and the wire feed speed to 4 m/mm. Due to the complexity of the part, the deposition had to be accomplished by combining different sections, except for deposition strategy 5 where additional material had to be added to avoid intersections. A distance of 3 mm was employed between the sections, as it provided a flat surface on the intersection.

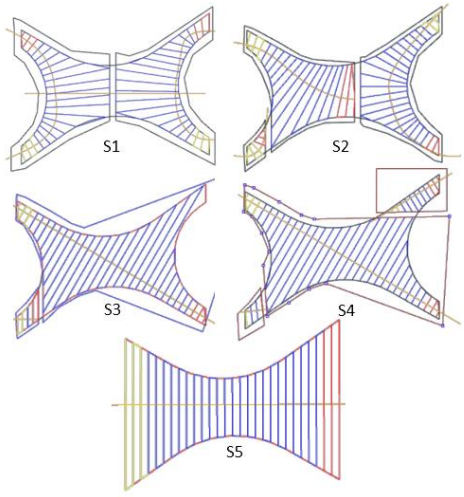

Figure 4 : Deposition strategies considered (S1-S5), numbered by deposition order of the sections.

3.3 Measurements acquired after the building process

Measurements of the layer heights were performed, using a calibrated height gauge. Samples of cross sections (cut as shown in Figure 5) for porosity analysis were made. The optical images were taken with a Nikon Optishot microscope at a magnification of 2.5 times and stitched together. The Vickers microhardness was measured using a Zwick Roell ZHV testing machine. In this test, the load of the diamond indenter was 100g and a dwell time of 15 seconds. The indentation points were executed as described in Figure 6. ARC-On and ARC-Off times were measured by a stop watch, in the same environment characteristics. The substrates' deformation analysis was carried out using a calibrated height gauge, measuring the difference of the highest point of deformation and the height of the substrate.

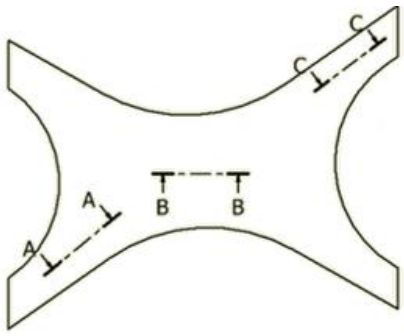

Figure 5 : Cut sections for the different deposition strategies. (a) For the strategies 1-4. For S5 the cuts were made in the same areas.

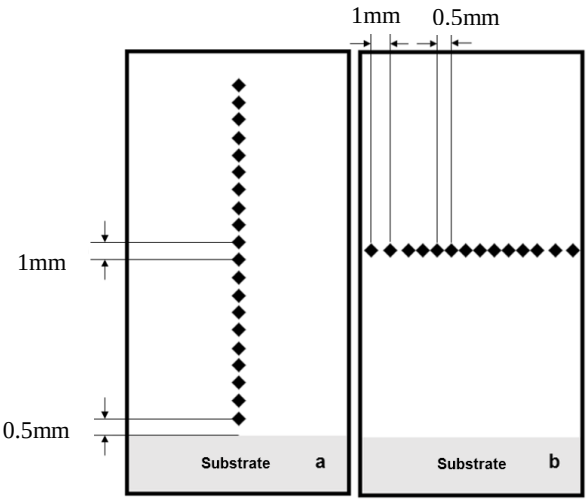

Figure 6 : Hardness test points. a) Vertical measurements and b) horizontal measurements. Figure not to scale.

4 RESULTS AND DISCUSSION

The successful strategies had the required height (above or close to 20mm) and didn't display any visual defect that would influence the part after machining (Figure 7). S2 presented a notorious lack of fusion in the last layer, resulting in the interruption of the deposition, not allowing the part to reach to the minimum of 20mm in height. Part S5 also presents a lack of fusion defect in the last layer. However, it was a result of the shift of the wire in the melt pool. Due to wire feedstock shortage, a re-do of the part wasn't possible.

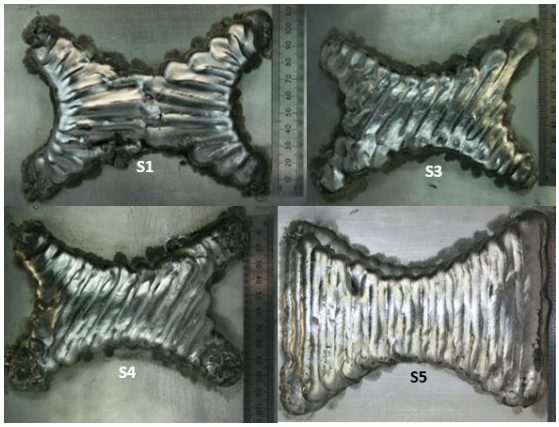

Figure 7 : Deposited parts with AA2319 as feedstock and AA6082 as build plate.

4.1 Pore distribution

Metallographic analyses of the different cuts were performed to compare the difference in pore size and distribution on the intersections and on the non-intersection areas. As the areas evaluated didn't have the same dimensions, the results are presented as average pore diameter, in micrometres, and the fraction area of the pores, in percentage Graph 1. Pores under 5 μm weren't optically visible and, therefore, aren't included in the results.

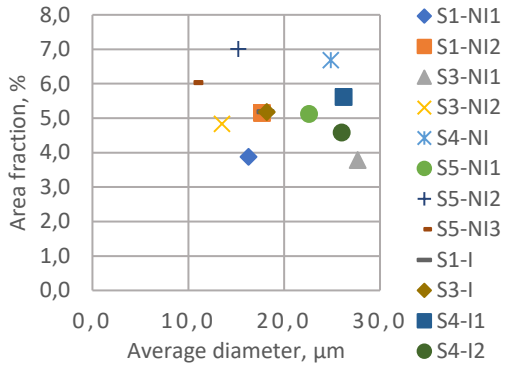

Graph 1: Pore area fraction by average pore diameter on the analysed sections.

By the analysis of Graph 1, it is possible to state that the higher average pore diameter is 27.7 µm and the lowest is 10.7µm. Furthermore, the obtained values vary in the same deposition strategy, with the highest difference for S3 strategy and smaller variation for S1 strategy.

Comparing both strategies, S1 is highly symmetric and the deposition is made more uniformly than for S3, assuring more similarly between the results. S5 displays the highest fraction of area, on average, comparing to the other deposition strategies, but the lowest in size diameter. The heat flow in this strategy is faster than the other deposition strategies, due to the highest surface area of the deposition (centre distance), resulting in a higher solidification rate, increasing the number of pores (as the pores don't have as much time to reach the surface) but with smaller diameter sizes due to the impediment of flowing to nucleate heterogeneity with other pores, forming larger ones. It is possible to state that an intersection, for the welding characteristics and parameters used, isn't a differentiating characteristic in terms of porosity area fraction nor pore average diameter.

4.2 Microhardness

Graph 2 presents the horizontal microhardness of the samples on the sectioned areas. By its analysis, the hardness values don't present a big variation, except for S4-I2, S1-NI2 and S3-NI1. This hardness augmentation may be associated with testing being held near or on a fusion line, as smaller grain sizes are predominant on that area, more grain boundaries will be inherent, inducing impediments to the movement of dislocations and increase the deformation resistance of the material.

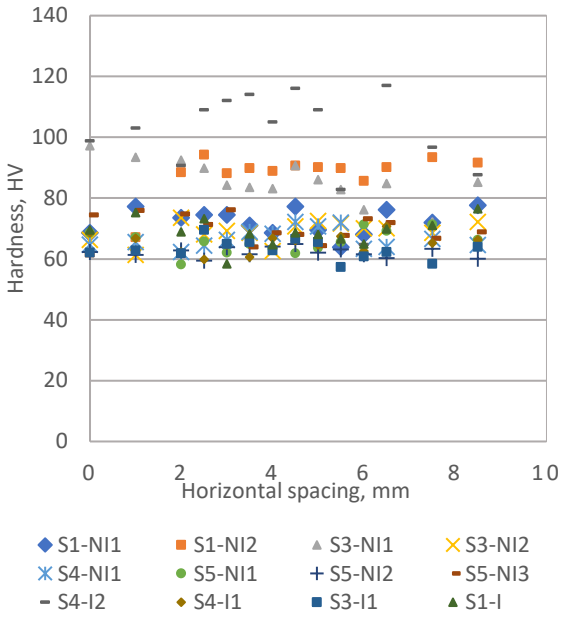

Graph 2 : Horizontal hardness comparison of the different deposition strategies.

Graph 3 describes the microhardness on the vertical direction of the B-B section of the S3 part. It is found that the microhardness values are similar amongst the deposition strategies, with values ranging between 81.2 HV to 63.1 HV for S1, between 76.9 HV to 62 HV for S3, 75.7 HV to 60.8 HV for S4 and 77.9 HV to 62.8 HV for S5. As S1 is characterized by an intersection in this section differing from the remaining strategies, it is possible to assume that the hardness is independent of this characteristic.

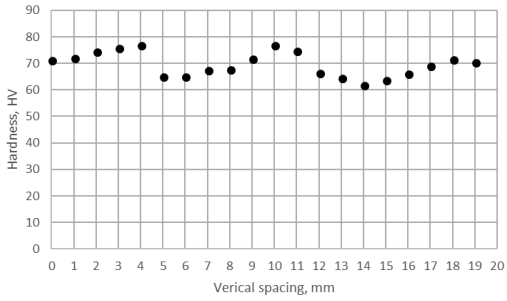

Graph 3 : Vertical hardness distribution of the deposition strategy 3.

Cong *et al.* [2] presented similar results by welding the same aluminium alloy in parallel deposition paths with CMT-ADV process but resulting with slight higher microhardness values. This issue may be related to the CMT characteristic of lower heat input when compared with ACPAW, which produces smaller grains, enhancing the microhardness results.

Derekar [42] showed in his work a maximum of approximately of 70 HV for an AA2319 alloy and Gu *et al.* [85] presented an average microhardness of 68.3 for CMT-PADV of AA2319 for single wall depositions on vertical measurements. The results are similar to the ones found in this research project.

4.3 Path efficiency and Substrate deformation

For every path programmed, the efficiency of the useful total time of the deposition (ratio between the arc-on/start and the total time to build a layer) was calculated using (1).

$$Path\ Efficiency = \frac{ARC - On\ time}{Total\ Time} * 100 \quad \textbf{(1)}$$

On Table 3, the results on the efficiency of the strategy deposition are displayed and, as expected, the efficiency of S5 is maximum as there's only one section in the part. For the nearest-shape deposition strategies, the most efficient is S3.

Table 3 : Deposition efficiency.

Deposition Strategy	**S1**	**S3**	**S4**	**S5**
Efficiency, %	96.7	97.3	94.4	100

The flatness of the surface was analysed by calculating the variance and the standard deviation of the height measurements of the final part. The result is related to the deposition efficiency as it describes how spread out the values are from the mean layer heights.

If the distance between the highest point and the lowest points are significant, the effective contact tip to work distance in the different zones will vary, potentially resulting in arc instability and more spatter.

Through Table 4 analysis, it is possible to conclude that the layer heights of S1 (followed by S5) are closer to the mean value, resulting in a smaller deviation in the height of the finished part. Per contra, there's a higher difference, on average, of the data collected and the mean value to the deposition strategies S3 and S4.

As distortions may be detrimental when considering the final dimensional accuracy of the part, they need to be taken into consideration.

Further analysis of Table 4 shows the substrate deformation for all the deposition strategies considered. It is notorious that the structure with the best performance on the matter is S5, with 1.39 mm of distortion. It may be related to the fact that the deposition is done in the most uniform and symmetric manner. As Ding *et al.* [9] stated and verified, a continuous path with one start and stop is preferred and more advantageous. It is also clear that the deposition pattern and sequence have an important role in the thermal history of the part.

Table 4 : Characteristics of the deposition strategies.

Deposition Strategy	**S1**	**S3**	**S4**	**S5**
Mean part height	19.8	23.78	23.7	23.8
Standard deviation	1.16	3.4	3.5	1.8
Substrate deformation	2.24	2.64	2.55	1.39

5 EVALUATION

The evaluation of the deposition characteristics was summarized in Table 5.

Table 5 : Evaluation of the different deposition strategies, considering its characteristics.

Deposition Strategy	***Evaluation***
S1	This deposition strategy excels in the flatness of the overall surface, even though it has an intersection; it produces the second smallest average pore diameter. However, it isn't recommended as it produced the smallest part average height, not reaching the desired 20mm and requiring an additional layer deposition.
S2	Unacceptable deposition strategy for this part construction due to deposition failure.
S3	Not suitable deposition strategy, as it induces the highest substrate deformation, has a high average pore diameter and a high standard deviation for part's height.
S4	Not recommended deposition strategy, as it produces the average largest pore diameters; has the lowest path efficiency, higher deviation of values in part height and induces the highest substrate deformation.
S5	Deposition strategy with the average smallest pore diameter; desirable 1 start/stop motion, guarantying a path efficiency of 100%; Only requires 4 layers, contrasting with other deposition strategies. Reaches the

Deposition Strategy	*Evaluation*
	highest part height and assures the lowest substrate deformation. However, the surface waviness on the sides has the highest values due to the programming mismatch and the deposition cost is almost 20% higher.

6 CONCLUSIONS

ACPAW process was successfully employed to produce five deposition strategies of a complex block aerospace part using AA2319 filler wire. The subsequent conclusions can be taken from this study project:

•Deposition strategies and its parameters are important to guaranty a deposition free of spatter and visual defects;

•Intersections study is outmost important, as they influence the arc stability and final characteristics of the constructed parts.

To propose the best the depositions strategy, a compromise between the data studied had to be accomplished. The deposition strategy chosen was S5 as it includes:

•One start/stop motion, producing a path efficiency of 100%, and a continuity of robot-deposition movement when fabricating the final aerospace part;

•Has the best part rate as only requires one less layer to achieve the desired final height;

•Even though the total cost is higher, the distortion of the substrate is the lowest of all the paths considered and the standard deviation of the height of the top surface showed an even surface, resulting in a good arc stability, increasing the process' automation;

•In a manufacturers' perspective, the porosity should be minimised, for strength enhancement. Therefore, the predominant factor choice was the average pore diameter, which revealed to the lowest for this deposition strategy.

REFERENCES

[1] F. Martina e S. Williams, "Wire+arc additive manufacturing vs. traditional machining from solid: a cost comparison," Cranfield University, 2015.

[2] I. Gibson, D. Rosen e B. Strucker, Additive manufacturing technologies - Rapid prototyping to direct digital manufacturing, Springer, 2010, pp. 21-.

[3] S. Williams, F. Martina, A. Addison, J. Ding, G. Pardal e P. Colegrove, "Wire+Arc Additive Manufacturing," *Materials Science and Technology,* pp. 642-647, 09 February 2016.

[4] "Weld metal composition change during conduction mode laser welding of aluminum alloy 5182," *Metallurgical and Materials Transactions B,* pp. 163-172, February 2001.

[5] H. Chen, "Process study of Al alloy WAAM with AC plasma," Cranfield university, 2016/17.

[6] Z. Pinter, "Study of Aluminium Wire + Arc Additive Manufacturing," Cranfield University, Master of Science thesis, 2017.

[7] G. Mathers, Welding of Aluminium and its alloys, CRC press, 2002, pp. 10-25.

[8] P. Vilaça, "Plasma Arc Welding," Materials Joining and NDT, Aalto University, 2015.

[9] D. Ding, Z. Pan, D. Cuiuri e H. Li, "Wire-feed additive manufacturing of metal components: technologies, developments and future interests," 23 March 2015.

[10] J. Ding, F. Martina e S. Wiliams, "Production of large metallic components by additive manifacture-Issues and achievements," *ResearchGate,* November 2015.

[11] P. Colegrove, A. McAndrew, J. Ding, F. Martina, P. Kurzynski e S. Williams, "System Architectures for Large Scale Wire + Arc Additive Manufacture," *10th*

International Conference on Trends in Welding Research, Japan, October 2016.

[12] G. Venturini, F. Montevecci, A. Scippa e G. Campatelli, "Optimization of WAAM deposition patterns for T-crossing features," *Optimization of WAAM deposition patterns for T-crossing features*, pp. 95-100, 2016.

[13] K. Ayarkwa, S. Williams and J. Ding, "Investigation of pulse advance cold metal transfer on aluminium wire arc additive manufacturing," *International Journal of Rapid Manufacturing,* vol. 5, pp. 44-58, 2015.

[14] Metals Handbook Desk Edition, ASM International, 1998.

[15] D. Ding, Z. Pan, D. Cuiuri e H. Li, "A multi-bead overlapping model for robotic wire and arc additive manufacturing (WAAM)," *Robotics and Computer-Integrated Manufacturing*, pp. 101-110, 2015.

[16] B. Cong, Z. Qi, B. Qi, H. Sun, G. Zhao e J. Ding, "A Comparative Study of Additively Manufactured Thin Wall and Block Structure with Al-6.3%Cu Alloy Using Cold Metal Transfer Process," *Applied Sciences,* vol. 7, p. 275, 10 March 2017.

[17] K. S. Derekar, "A review of wire arc additive manufacturing and advances in wire arc additive manufacturing of aluminium," *Materials Science and Technology*, 08 April 2018.

[18] J. Gu, B. Cong, J. Ding, S. Williams e Y. Zhai, "Wire + Arc Additive Manufacturing of Aluminium," em *Solid freeform fabrication symposium*, Austin, Texas, 2014.

[19] CUI INC, "Design considerations for thermal management of power supplies," 11 2014. [Online]. Available: https://www.cui.com/catalog/resource/design-considerations-for-thermal-management-of-power-supplies.pdf. [Acedido em 07 April 2018].

[20] F. Martina, J. Mehnen, S. Williams, P. Colegrove e F. Wang, "Investigation of the benefits of plasma deposition for the additive layer," *Journal of Materials Processing Technology*, pp. 1377-1386, 2012.

[21] E. Gharibshahiyan, A. H. Raouf, N. Parvin e M. Rahimian, "The effect of microstructure on hardness and toughness of low carbon welded steel using inert gas welding," *Materials and Design*, pp. 2042-2048, 2011.